

Grant-Free Transmission by LDPC Matrix Mapping and Integrated Cover-MPA Detector

Linjie Yang, *Student Member, IEEE*, Pingzhi Fan, *Fellow, IEEE*,
Li Li, *Member, IEEE*, Zhiguo Ding, *Fellow, IEEE*, Li Hao, *Member, IEEE*

Abstract

In this paper, a novel transceiver architecture is proposed to simultaneously achieve efficient random access and reliable data transmission in massive IoT networks. At the transmitter side, each user is assigned a unique protocol sequence which is used to identify the user and also indicate the user's channel access pattern. Hence, user identification is completed by the detection of channel access patterns. Particularly, the columns of a parity check matrix of low-density-parity-check (LDPC) code are employed as protocol sequences. The design guideline of this LDPC parity check matrix and the associated performance analysis are provided in this paper. At the receiver side, a two-stage iterative detection architecture is designed, which consists of a group testing component and a payload data decoding component. They collaborate in a way that the group testing component maps detected protocol sequences to a tanner graph, on which the second component could execute its message passing algorithm. In turn, zero symbols detected by the message passing algorithm of the second component indicate potential false alarms made by the first group testing component. Hence, the tanner graph could iteratively evolve. The provided simulation results demonstrate that our transceiver design realizes a practical one-step grant-free transmission and has a compelling performance.

Index Terms

Grant-Free, Short-Packet-Transmission, Group Testing, Cover Decoder, Iterative Detection.

Linjie Yang, Pingzhi Fan, Li Li, and Li Hao are with the School of Information Science and Technology, Southwest Jiaotong University, Chengdu 610031, China (e-mail: yanglinjie@my.swjtu.edu.cn; pzf@swjtu.edu.cn; ll5e08@home.swjtu.edu.cn; lhao@swjtu.edu.cn).

Zhiguo Ding is with the Department of Electrical Engineering, Princeton University, Princeton, NJ 08544 USA, and also with the Department of Electrical and Electronic Engineering, The University of Manchester, Manchester M13 9PL, U.K. (e-mail: zhiguo.ding@manchester.ac.uk).

I. INTRODUCTION

Massive machine type communication (mMTC) has attracted comprehensive research interests in recent years, since it was identified as one of the three major services of the fifth generation mobile communication (5G) system. Especially, after the freeze of 3GPP release-16 [1], the requirements of enhanced mobile broadband communications (eMBB) had been well satisfied. Hence, researchers turn to dedicate efforts to solve the challenges for the implementation of mMTC. The mMTC service has its particular features: (1) compared with human-to-human (H2H) communications, the number of potential users (devices) in mMTC scenario could reach up to millions per km^2 [2]; (2) the user activity patterns are very sporadic; (3) mMTC demonstrates a salient short-packet-transmission property [3]; (4) the users are very sensitive to energy consumption [4]. As a result, employing traditional four-step random access in mMTC scenarios will induce a challenging overhead problem that typically, hundreds of signaling bits are transmitted for facilitating the transmission of just several payload bits. Among the solutions of this high overhead problem, grant-free (GF) random access (RA) is a promising candidate which aims at implementing the synchronization, active user identification, channel estimation, as well as the data recovery in a one-shot joint operation [5]. Currently, compressive sensing (CS) based GF RA [6]–[8], unsourced random access (URA) [9]–[13] and GF non-orthogonal multiple access (GF-NOMA) [14]–[18] constitute main GF techniques.

Most of the existing CS based GF RA schemes leverage the particular feature of mMTC users that they normally access the channel in a sporadic manner. Hence, the active user identification and channel estimation engaged in RA process could be accomplished by CS technologies. In more depth, depending on the number of antennas deployed at the BS, they could be formulated to either a single measurement vector problem [6] or a multiple measurement vector problem [8]. It was also demonstrated in [6] and [7] that the approximate message passing (AMP) algorithm contributes an efficient solution of these problems. While further considering the data transmission, Larrson *et al.* developed the prototype in [6], [7] by embedding user data bits directly in its optional random access preambles. Hence, a one-step GF transmission framework is realized in [8]. But, the number of data bits that could be afforded by this framework is quite small, e.g., several bits per user. Hence, designing a practical one-step GF transmission framework is still an important open problem.

URA technologies pave another way to approaching one-step GF transmission. Polyanskiy *et al.* firstly proposed the URA concept [9] by regarding the active user identification and data recovery as a fundamental coding problem. In [9], all the users employ the same codebook, where user identity is regarded as a part of entire data bits and the theoretical performance bound of URA framework is derived. Polyanskiy *et al.* also exhibited a practical realization of the framework in [10], which was referred as T-fold ALOHA. A two-stage receiver consisting of outer and inner coding components plays a critical role in T-fold ALOHA. A two-stage receiver architecture was employed in ensuing developments of URA technology [11]–[13], where the first stage is for user identification while the second stage is for data recovery. Compared with [10], more sophisticated anti-jamming techniques were proposed for GF in [11]–[13].

The development of NOMA technology paralleled the explosion of IoT devices, since it can support severely overloaded communication, where the number of active users significantly exceeds that of channel resources. After abandoning the idealized assumption that BS always has a prior knowledge of user-activity, GF NOMA technologies occurred. Accordingly, they focused on solving active user identification before implementing non-orthogonal multiple access. Dynamic compressive sensing, subspace pursuit as well as orthogonal matching pursuit algorithms were developed in [14]; Golay complementary sequence is employed as a new kind of preamble in [15]; a two-stage receiver realizing joint user-activity and data detection is designed for NOMA uplink in [16].

The mechanism that an active user needs to send a user-specific preamble to facilitate its identification at BS is adopted in most of the aforementioned GF RA frameworks. Benefiting from the intrinsic sparsity of the massive IoT network and leveraging the advanced CS technologies, the preamble length required by them has been significantly less than that required by conventional orthogonal RA under the constraint of achieving the same RA success probability. However, normally, the preamble is till extremely longer than data stream due to the short-packet-transmission property of IoT users.

In order to essentially solve the overhead problem caused by directly sending preambles to distinguish users, the literatures [19]–[21] alternatively embed user identity in its channel access pattern. To be more concrete, the same data packet of a user will be repeated on multiple channel resources. The distribution of these loaded channel resources is termed the user channel access

pattern. Hence, it is feasible to establish one-to-one mapping between the user identity and channel access pattern. Furthermore, the channel access pattern of active users can be detected by the group testing (GT) algorithm [21]. However, currently, the performance of group testing is still constrained by the active user sparsity. It works well only in extremely sparse scenario. How to coordinate the channel access patterns of all the coexisted users for supporting more simultaneously activated users is still an important open problem [22], [23]. In [24], a more radical solution was proposed, which even did not have an explicit active user identification stage. Its message passing algorithm based receiver directly decodes the transmitted symbol of every coexisted users. Particularly, it adds zero symbols to the search space. If the transmitted symbol of a user is decoded as zero, it will be regarded as an inactive user. Apparently, the complexity of this solution rapidly becomes prohibitive upon increasing the number of coexisted users. Furthermore, in [25], a novel GF low-density-signature orthogonal frequency division multiplexing (GF LDS-OFDM) is proposed, where its joint active user identification and channel estimation (CE) is realized without using preamble. In contrast, its joint active user identification and CE is formulated as an estimation problem of structural signals, and message passing based Bayesian algorithms are employed to solve this estimation problem. However, it does not has any information exchange mechanism to further justify or correct the user identification results. Again, unfortunately, its performance will degrade dramatically with the growth of user sparsity.

In order to improve the above-stated one-step GF short-packet-transmission, which avoids explicit preamble transmissions, we propose a novel transceiver architecture, whose main contributions are summarized as follows.

- A novel GF short-packet transmission scheme is proposed, where the active user identification and data decoding is realized jointly without using preamble. At the transmitter side, inspired by [21], the user identity is bound to its channel access pattern, which is indicated by a binary protocol sequence. A coordinated construction of the overall protocol sequence set is realized by mapping columns of a proper LDPC parity check matrix to the protocol sequences.
- At the receiver side, a two-stage iterative detection architecture is designed, which consists of a group testing component and a payload data decoding component. The first-stage group testing component maps its detected protocol sequences to a tanner graph, on which the

second-stage data decoding component could execute its message passing algorithm. In the initial iteration, the cover decoder serves as our group testing algorithm to overcome the absence of the prior knowledge from the data decoding component. After the initial iteration, the cover decoder is replaced iteratively by a simple belief propagation (BP) algorithm, which converts zero symbol probabilities fed back from the data decoding component to the user activity states. Hence the potentially redundant nodes could be pruned from previous tanner graph used in the data decoder. In this manner, the receiver performance could be iteratively improved.

- The design guideline of the aforementioned LDPC parity-check-matrix based user specific protocol sequences is provided, which appropriately couples with the decoding rule of cover decoder that employed at the first detection stage. Accordingly, the optimization of its LDPC parity-check-matrix is discussed. Moreover, the computational complexity of the proposed two-stage iterative detection algorithm is also analyzed.

The rest of this paper is organized as follows. The system model is described in Section II. The work of the group testing component and the data decoding component are discussed in Section III and Section IV respectively. Simulation results is presented in Section V. The paper is concluded in Section VI.

Notations : In this paper, \mathbf{S}^H denotes the conjugate transpose of matrix \mathbf{S} . $\mathbf{S}[:, \mathcal{U}]$ consists of a set of columns in \mathbf{S} , whose indices are given in \mathcal{U} . $|\mathcal{A}|$ denotes the number of elements in the set \mathcal{A} . $\|\cdot\|_p$ denotes the l_p -norm.

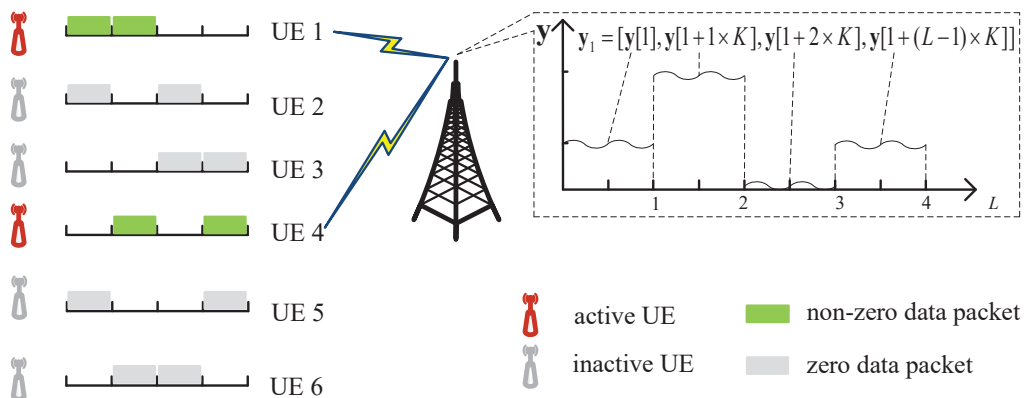


Fig. 1: The proposed one-step grant-free uplink transmission framework.

II. SYSTEM MODEL

In this section, the system model of our one-step GF short-packet-transmission is elaborated. The important assumptions adopted in our system are emphasized first.

We focus on the uplink of a single IoT cell. We assume that a number of N users coexist in the cell, among which, a number of N_a users will independently wake up and send data in once GF transmission period. Accordingly, the cellular user sparsity is defined as $\lambda = \frac{N_a}{N}$. During one random access procedure, a total number of L channel resources are available for carrying all uplink transmissions of active users. Without loss of generality, L uniform time-slots are considered in this paper and each of them has the same length as a data-packet¹. For simplifying the signaling and analysis, we further assume the system always achieves an idealized symbol-wise synchronization and experiences AWGN channels. Normally, the IoT devices are low-cost and energy constrained, which motivates the used assumption that a single antenna is deployed in both the user and the BS.

Each cellular user u is assigned with a unique protocol sequence $\mathbf{s}_u \in \mathbb{B}^{L \times 1}$, $u = 1, 2, \dots, N$. As addressed in Section I, \mathbf{s}_u can also be termed as the channel access pattern of user u . A user u generates its original alphabet \mathcal{X}_u according to [26], where each standard M -ary phase shift keying (PSK) symbol is further multiplied by a user-specific complex coefficient. Then, similar to the sparse CDMA system discussed in [24], an extra zero constellation point is added to its original alphabet for exposing its inactive state at BS. Hence, the final alphabet of user u has a cardinality of $|\mathcal{X}_u| = \mathcal{M} + 1$, $u = 1, 2, \dots, N$.

When the one-step GF transmission of a user u commences, it firstly switches its activity state from $a_u = 0$ to $a_u = 1$. Then, its data packet of length K , $\mathbf{x}_u = [x_u[1], x_u[2], \dots, x_u[K]]^T \in \mathbb{C}^{K \times 1}$ is prepared, whose component symbols $x_u[k]$, $k = 1, 2, \dots, K$, are selected from \mathcal{X}_u . Subsequently, the data packet \mathbf{x}_u is spread by its protocol sequence \mathbf{s}_u in the form of $\mathbf{x}_u^c = \mathbf{s}_u \otimes \mathbf{x}_u \in \mathbb{C}^{KL \times 1}$, where \otimes denotes the Kronecker product and \mathbf{x}_u^c denotes the spread data-packets of user u .

Assuming all the active users are perfectly aligned in time, the signal sequence received at

¹ Alternatively, they could be L uniform sub-bands in the frequency domain.

the BS during a single GF transmission period is given by

$$\mathbf{y} = \sum_{u=1}^N \mathbf{x}_u^c \cdot a_u + \mathbf{n}. \quad (1)$$

Then, by sampling \mathbf{y} at k^{th} symbol duration of every time-slot and assembling these L samples, we glean the k^{th} sub-vector of \mathbf{y} , which could be formulated as

$$\begin{aligned} \mathbf{y}_k &= \sum_{u=1}^N a_u [\mathbf{x}_u^c[k], \mathbf{x}_u^c[k + K \cdot 1], \dots, \mathbf{x}_u^c[k + K(L - 1)]]^T + \mathbf{n}_k \\ &= \mathbf{S}\mathbf{X}_k\mathbf{a} + \mathbf{n}_k, \end{aligned} \quad (2)$$

where $\mathbf{S} = [\mathbf{s}_1, \mathbf{s}_2, \dots, \mathbf{s}_N] \in \mathbb{B}^{L \times N}$. $\mathbf{X}_k = \text{diag}(x_1[k], x_2[k], \dots, x_N[k]) \in \mathbb{C}^{N \times N}$, $\mathbf{a} = [a_1, a_2, \dots, a_N]^T$, and \mathbf{n}_k is an $L \times 1$ Gaussian vector, whose element follows an i.i.d distribution of $\mathcal{CN}(0, \delta^2)$.

An example of our considered one-step GF uplink transmission framework is illustrated in Fig. 1, where $N = 6$ IoT users coexist in the cell and $L = 4$ time-slots are employed for a single GF transmission period. Hence, the length of protocol sequence $\mathbf{s}_u, u = 1, \dots, 6$ is also fixed to $L = 4$. On the left-hand side of Fig. 1, \mathbf{s}_u is directly visualized by channel access pattern of user u , whose non-zero element indicates at which time-slot a data packet should be loaded, e.g. $\mathbf{s}_1 = [1, 1, 0, 0]$. Assume a pair of symbols are delivered in one time slot, i.e. $K = 2$, the data packet of user 1 could be formulated as $\mathbf{x}_1 = [x_1[1], x_1[2]]^T$. After spreading \mathbf{x}_1 by \mathbf{s}_1 , user 1 sends its entire signal frame $\mathbf{x}_1^c = [x_1[1], x_1[2], x_1[1], x_1[2], 0, 0, 0, 0]^T$. Assume that user 1 and 4 are active, other users are asleep, according to (2), the 1^{st} sub-vector of received signal sequence is given by

$$\begin{bmatrix} y[1] \\ y[3] \\ y[5] \\ y[7] \end{bmatrix} = \begin{bmatrix} 1 & 1 & & 0 \\ 1 & 0 & \dots & 1 \\ 0 & 1 & & 1 \\ 0 & 0 & & 0 \end{bmatrix} \cdot \begin{bmatrix} x_1[1] & & & & & & & \\ & x_2[1] & & & & & & \\ & & \ddots & & & & & \\ & & & & & & & x_6[1] \end{bmatrix} \cdot \begin{bmatrix} 1 \\ 0 \\ 0 \\ 1 \\ 0 \\ 0 \\ 0 \\ 0 \end{bmatrix} + \mathbf{n}_1, \quad (3)$$

III. ACTIVE USER IDENTIFICATION

The Message passing algorithm (MPA) was leveraged in [27] to recover multi-user symbols from the superposed signals, e.g. from \mathbf{y}_k given in (2). Its key idea is representing the channel

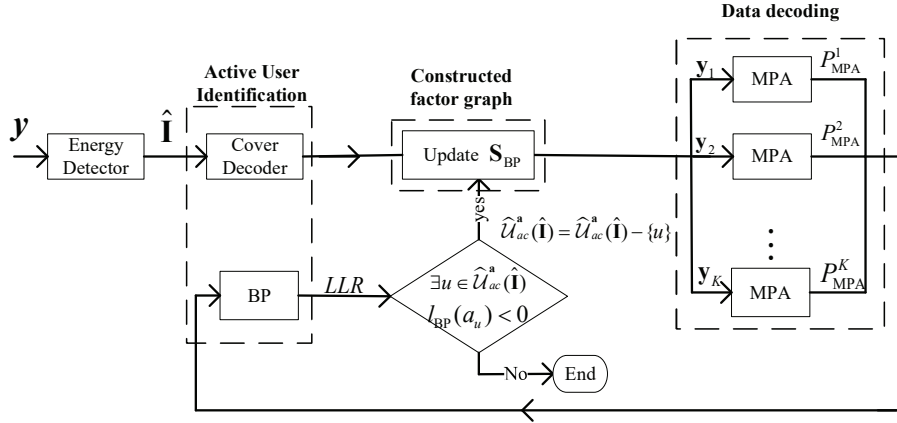


Fig. 2: Schematic of the proposed two-stage iterative active user identification and data recovery.

access patterns of all users in a form of the LDPC parity-check matrix, e.g. the matrix \mathbf{S} in (2). Hence, the factor graph required by the MPA algorithm is obtained according to \mathbf{S} . This scheme was adopted as a fundamental technology in many NOMA systems [28], [29]. However, it cannot be directly applied to our case owing to the fact that N is normally quite large in mMTC scenario. The extremely high dimensionality of \mathbf{S} will impose prohibitive complexity on MPA. Hence, we have to implement active user identification before data recovery. Accordingly, the columns² $s_n, n \in \mathcal{U}_{ina}$ can be removed from \mathbf{S} . This pruned \mathbf{S} will significantly reduce the computing complexity of MPA and mitigate the distortion caused by false-alarmed users as well.

Inspired by [21], again, active user identification is regarded as a group testing problem in this paper. But its performance is improved by us through two aspects: a) instead of disjunct matrices [22], [23], the protocol sequence used in the cover decoder which is obtained from a properly constructed LDPC parity-check matrix; b) not only the cover decoder but also the belief propagation (BP) decoder are employed in group testing procedure, where the later enable the receiver to iteratively update \mathbf{S} based on the feedbacks from data decoder.

A. General Principle of Cover Decoder

Let \mathbf{I} denote the load states of each time-slot during one GF transmission. If data packets of any active user are transmitted on l^{th} time-slot, we have $\mathbf{I}[l] = 1$, otherwise, $\mathbf{I}[l] = 0$. According

² \mathcal{U}_{ina} is the set of asleep users.

to these definitions, \mathbf{I} is determined by

$$\mathbf{I} = \bigvee_{u \in \mathcal{U}_{ac}^{\mathbf{a}}} \mathbf{s}_u, \quad (4)$$

where $\mathcal{U}_{ac}^{\mathbf{a}} = \{u | \mathbf{a}[u] = 1, 1 \leq u \leq N\}$ indicates the set of active users and \bigvee denotes Boolean-OR operation of vectors. Obviously, $\mathcal{U}_{ac}^{\mathbf{a}}$ is determined by its superscript \mathbf{a} , which is defined in (2).

The cover decoder completes its active user identification through three steps:

- Firstly, load state \mathbf{I} is detected as $\hat{\mathbf{I}}$ by energy detector, which will be addressed in Section II.C.
- Secondly, according to the distribution of zero elements in $\hat{\mathbf{I}}$, the set of inactive users $\mathcal{U}_{ina}^{\mathbf{a}}$ can be estimated.
- Finally, assuming that $\mathcal{U}_{ina}^{\mathbf{a}}$ has been estimated as $\hat{\mathcal{U}}_{ina}^{\mathbf{a}}(\hat{\mathbf{I}})$, the set of active users $\mathcal{U}_{ac}^{\mathbf{a}}$ is simply estimated by its complementary set of $\hat{\mathcal{U}}_{ac}^{\mathbf{a}}(\hat{\mathbf{I}}) = \mathcal{U} - \hat{\mathcal{U}}_{ina}^{\mathbf{a}}(\hat{\mathbf{I}})$.

Take Fig. 1 as an example again. According to the channel load states depicted on the top-right corner of Fig. 1, we assume perfect load state estimation, i.e. $\hat{\mathbf{I}} = \mathbf{I} = [1, 1, 0, 1]$. The zero element on the third index of \mathbf{I} determines whether it is possible that a user whose channel access pattern occupies the third time-slot is an active user during current GF transmission. Hence, the set of inactive users is estimated as $\hat{\mathcal{U}}_{ina}^{\mathbf{a}}(\mathbf{I}) = \{2, 3, 6\}$. Accordingly, the set of active users is estimated as $\hat{\mathcal{U}}_{ac}^{\mathbf{a}}(\mathbf{I}) = \{1, 4, 5\}$. Obviously, in this case, $\hat{\mathcal{U}}_{ac}^{\mathbf{a}}(\mathbf{I})$ is not completely identical to $\mathcal{U}_{ac}^{\mathbf{a}}$, which does not include user 5. This problem could be solved by the proposed two-stage iterative detection architecture as shown in Fig. 2.

Furthermore, based on $\hat{\mathcal{U}}_{ac}^{\mathbf{a}}(\hat{\mathbf{I}})$, we can obtain the spreading matrix of active users $\mathbf{S}[:, \hat{\mathcal{U}}_{ac}^{\mathbf{a}}(\hat{\mathbf{I}})]$, which could be converted to a factor graph by regarding its columns as variable nodes and rows as check nodes.

B. Protocol Sequence Design for Cover Decoder

As suggested in [27], in order to guarantee the efficiency of MPA, the users' spreading sequences should be sparse. As a result, the spreading matrix generated in [27], which plays a similar role as our \mathbf{S} in (2), is a sparse matrix and hence may be regarded as an LDPC parity check matrix. This fact inspires us to map an LDPC parity check matrix to our spreading matrix

S. The results in [27] show that most LDPC parity check matrices, even those have short cycles, are suitable for the LDS scheme. However, in our case, the active user identification performance will demonstrate noticeable variation while assigning different LDPC parity check matrices to \mathbf{S} and using the cover decoder. Hence, optimizing the LDPC parity check matrix employed in cover decoder algorithm is of great importance.

Spreading matrix optimization in the background of cover decoder applications has been studied in [22], [23], where it was also termed the non-adaptive group testing (GT) problem. Moreover, in these studies, a noiseless case where $\hat{\mathbf{I}} = \mathbf{I}$ is assumed in the optimization process of the spreading matrix. It was proved in [22], [23] that in order to minimize the active user identification error, which could be quantified by $|\hat{\mathcal{U}}_{ac}^{\mathbf{a}}(\mathbf{I}) - \mathcal{U}_{ac}^{\mathbf{a}}|$, spreading matrix has to be a disjunct matrix. With the aid of the disjunct matrix based design of spreading matrix, error-free active user identification becomes possible. However, the penalty is that the user activity pattern of a mobile-cell has to be extremely sparse, i.e. the parameter λ has to be extremely small. Otherwise, the active user identification error will dramatically increase.

Proposing such a solution of GT problem in [22], [23] is owing to an underlying constraint that they have to accomplish active user identification in once chance, i.e. only through the cover decoder. But now, in our proposed two-stage iterative detection architecture, the false alarm made in the cover decoder could be corrected by detecting zero symbols during the ensuing data recovery stage. Hence, it is no longer necessary to pursuit perfect active user identification of the cover decoder. This relax of $|\hat{\mathcal{U}}_{ac}^{\mathbf{a}}(\mathbf{I}) - \mathcal{U}_{ac}^{\mathbf{a}}|$ during the cover decoder stage brings us two benefits: 1) the performance of active user identification can remain at an acceptable level in a wider range of λ ; 2) the spreading matrix is not necessary to be a disjunct matrix, which means that other construction methods, e.g. employing an LDPC parity check matrix, becomes feasible.

Based on above analysis, we propose that the spreading matrix of all coexisted users \mathbf{S} should result in two properties:

$$\mathcal{U}_{ac}^{\mathbf{a}} \subseteq \hat{\mathcal{U}}_{ac}^{\mathbf{a}}(\mathbf{I}), \quad (5)$$

$$R_{\text{FA}} = \frac{\sum_{\substack{\mathbf{a} \in \mathbb{B}^{N \times 1} \\ \|\mathbf{a}\|_0 = \lambda N}} |\hat{\mathcal{U}}_{ac}^{\mathbf{a}}(\mathbf{I}) - \mathcal{U}_{ac}^{\mathbf{a}}|}{\sum_{\substack{\mathbf{a} \in \mathbb{B}^{N \times 1} \\ \|\mathbf{a}\|_0 = \lambda N}} |\mathcal{U}_{ac}^{\mathbf{a}}|} \leq \tau. \quad (6)$$

where $\|\cdot\|_0$ denotes l_0 -norm. Determined by the decoding principle of the cover decoder, the requirement of (5) is always achievable as long as the load state \mathbf{I} is perfectly estimated [22], [23]. The threshold τ in (6) specifies the maximum false alarm that is allowed in the cover decoder. If τ is set too large, the data decoding component illustrated in Fig. 2 will suffer from an extremely high decoding complexity. In turn, a very low false alarm level τ is only possible in a very sparse user access pattern, i.e. the number of active users has to be seriously limited. According to [30], without the *a priori* knowledge of sparsity λ , the cardinality of $\hat{\mathcal{U}}_{ac}^a(\mathbf{I})$ may exceed twice or even triple of \mathcal{U}_{ac}^a . Hence, in order to constrain the tanner graph size used later by the MPA algorithm and simultaneously afford more active users, $R_{FA} \leq 1$ is pursued in our design.

Proposition 1. *By employing a regular LDPC parity check matrix having column weight w_c , number of rows L , number of columns N and girth larger than 4 as the spreading matrix \mathbf{S} . Assume the load states \mathbf{I} is perfectly estimated. The false alarm performance R_{FA} of cover decoder will be a function of λ , r and w_c as follows*

$$R_{FA}(\lambda, w_c, r) = \frac{1 - \lambda}{\lambda} (1 - (1 - \lambda)^{\frac{w_c}{r} - 1})^{w_c}, \quad (7)$$

Proof: See Appendix A. ■

It is well known that massive IoT networks are typical energy constrained and channel resource limited communication scenarios [10], [21]. Hence, the column weight w_c , which is equivalent to the repeat times of a data packet, should be as small as possible to save transmission energy. In the same spirit, the ratio of $r = \frac{L}{N}$, which is equivalent to the number of channel resources per cellular user required should also be as small as possible. Based on these analysis and Proposition 1, optimizing the spreading matrix \mathbf{S} becomes tractable and could be formulated as a multi-objective optimization problem [31].

$$\begin{aligned} \min_{w_c, r} \quad & [w_c, r] \\ \text{s.t.} \quad & C_1 : w_c \geq 2 \\ & C_2 : 0 < r < 1 \\ & C_3 : R_{FA}(\lambda^*, w_c, r) \leq \tau \end{aligned} \quad (8)$$

where λ^* is the specific value of λ , which maximizes R_{FA} after w_c and r are given. C_1 comes from the constraint of the column weight used in regular LDPC parity check matrices. C_2 comes from the fact that we focus on an overloaded communication system, and C_3 is added for satisfying (6).

Directly obtain the optimum solution of w_c based on its original formulations in (8) is quite difficult. Its major challenge is the monotonicity of $R_{\text{FA}}(\lambda^*, w_c, r)$ with respect to w_c is unknown. In order to circumvent this problem, the constraint C_3 that $R_{\text{FA}}(\lambda^*, w_c, r) \leq \tau$ may be replaced by requiring the upper bound of $R_{\text{FA}}(\lambda^*, w_c, r)$ to be less or equal than τ . Obviously, this replacement tightens previous constraint C_3 , but we could prove later that it will not modify the optimum w_c .

According to the above-mentioned clarification, the upper bound on $\ln R_{\text{FA}}(\lambda, w_c, r)$ is given by

$$\ln(R_{\text{FA}}(\lambda, w_c, r)) \leq \ln\left(\frac{1-\lambda}{\lambda}\right) - w_c(1-\lambda)^{\frac{w_c}{r}-1}, \quad (9)$$

where the inequality of $\ln(1-x) \leq -x$, $x \in (0, 1)$ is employed. $R_{\text{FA}}(\lambda, w_c, r)$ is substituted as $1-x$. Let $g(\lambda, w_c, r)$ represent the upper bound $\ln\left(\frac{1-\lambda}{\lambda}\right) - w_c(1-\lambda)^{\frac{w_c}{r}-1}$. Consequently, constraint C_3 could be replaced by $g(\lambda, w_c, r) \leq \ln \tau$. As a result, the optimization problem in (8) is transformed to

$$\begin{aligned} \min_{w_c, r} \quad & [w_c, r] \\ \text{s.t.} \quad & C_1 \sim C_2, \\ & C_4 : g(\lambda^*, w_c, r) \leq \ln \tau \end{aligned} \quad (10)$$

Proposition 2. *By employing a regular LDPC parity check matrix, having column weight w_c , number of rows L , number of columns N and girth larger than 4 as the spreading matrix \mathbf{S} , $g(\lambda^*, w_c, r)$ will be a monotonically increasing function of w_c for any given r .*

Proof: See Appendix B. ■

Based on Proposition 2, it is possible to show whether the optimization object formulated in (8) or that formulated in (10) will result in the same optimum solution of $w_c = 2$. More details can be found in Appendix C.

Proposition 3. *By employing a regular LDPC parity check matrix, having column weight w_c ,*

number of rows L , number of columns N and girth larger than 4 as the spreading matrix \mathbf{S} , $R_{\text{FA}}(\lambda, w_c, r)$ will be a monotonically decreasing function of r for any given λ and w_c .

Proof: See Appendix D. ■

After substituting $w_c = 2$ into constraint C_3 , the original optimization object given in (8) can be simplified as (11).

$$\begin{aligned} \min_r \quad & r \\ \text{s.t.} \quad & C_2, \\ & R_{\text{FA}}(\lambda^*, 2, r) \leq \tau \end{aligned} \tag{11}$$

Apparently, based on Proposition 3, the optimization problem in (11) is tractable and the optimum solution of r , namely r^* is determined by τ . The value of r^* with several typical τ are listed in TABLE I.

TABLE I: r^* with different τ

τ	0.5	1	1.5	2
r^*	0.6666	0.5	0.4	0.31

C. Energy Detector

Both the cover decoder and BP decoder are employed for active user identification. Their implementation requires the knowledge of load states of all time-slots, i.e. \mathbf{I} . In order to simplify the numerical analysis in Section III.B, it is assumed that \mathbf{I} is perfectly known at the receiver side. However, in practice, the estimation of \mathbf{I} is still necessary. Inspired by [32], an energy threshold based load state estimator is proposed.

In particular, the entire energy of the received packet on the l^{th} time-slot is given by

$$E_l = \sum_{k=1}^K |\mathbf{y}[k + K(l-1)]|^2 = \sum_{u=1}^N a_u \|\mathbf{x}_u\|_2 + K\delta^2. \tag{12}$$

In the estimation process of \mathbf{I} , if the entire energy received on a time slot exceeds a predefined threshold τ_E , this time slot will be marked as loaded, i.e. we have $\mathbf{I}[l] = 1$ if $E_l \geq \tau_E$. Otherwise, $\mathbf{I}[l] = 0$.

D. BP algorithm based active user identification

As introduced in Section II, an extra zero symbol is added to alphabet \mathcal{X}_u of each user for indicating its asleep state. Hence, the BP algorithm has an ability to correct some false alarms that were made by the cover decoder in the first round of active user identification. The principle is simply that if the probability of $P\{a_u = 0\}$ calculated by BP algorithm is sufficiently high, the BP algorithm will assign $a_u = 0$ and the u^{th} user is removed from the estimated active user set $\hat{\mathcal{U}}_{ac}^a(\hat{\mathbf{I}})$.

In particular, the BP algorithm will iteratively execute (13) and (14) T times and then make its final estimation of $P\{a_u = 0\}$.

$$E_{c \rightarrow v}^{(i)} = \log\left(\frac{1}{1 - \prod_{v' \in \mathcal{N}(c) \setminus \{v\}} (1 + \exp(E_{v' \rightarrow c}^{(i-1)}))^{-1}}\right), \quad (13)$$

$$E_{v \rightarrow c}^{(i)} = l_{\text{MPA}}(a_v) + \sum_{c' \in \mathcal{N}(v) \setminus \{c\}} E_{c' \rightarrow v}^{(i-1)}, \quad (14)$$

where c and v represent check node and variable node of a factor graph, respectively. This factor graph is transformed from the spreading matrix \mathbf{S} that defined in (2). To be more specific, only the columns whose indices are included in $\hat{\mathcal{U}}_{ac}^a(\hat{\mathbf{I}})$ are remained, hence \mathbf{S} is reduced to $\mathbf{S}[:, \hat{\mathcal{U}}_{ac}^a(\hat{\mathbf{I}})]$. All zero rows in $\mathbf{S}[:, \hat{\mathcal{U}}_{ac}^a(\hat{\mathbf{I}})]$ are further removed, and resultant matrix could be denoted by \mathbf{S}_{BP} . Based on \mathbf{S}_{BP} , the factor graph is obtained by regarding its rows (i.e. time-slots) as check nodes and its columns (i.e. user activity state) as variable nodes. Hence, we have $c \in \{l | \mathbf{I}[l] = 1\}$ and $v \in \hat{\mathcal{U}}_{ac}^a(\hat{\mathbf{I}})$. Then, $\mathcal{N}(c)$ denotes the set of variable nodes that are connected with the check node c on the factor graph. $\mathcal{N}(c) \setminus \{v\}$ means remove the variable node v out of $\mathcal{N}(c)$. Furthermore, $l_{\text{MPA}}(a_v)$ is the *a priori* information of the activity state a_v , which is provided by the data decoding component in Fig. 2. Moreover, $E_{c \rightarrow v}^{(i)}$ is the extrinsic information transferred from check node c to variable node v within the i^{th} iteration. Particularly, $E_{v \rightarrow c}^{(i)} = 0$ for $i < 0$, and hence $E_{v \rightarrow c}^{(0)} = l_{\text{MPA}}(a_v)$.

Accordingly, at the last iteration, BP algorithm will output the log-likelihood ratio (LLR) of activity state a_v as follows

$$l_{\text{BP}}(a_v) = \log\left(\frac{P(a_v = 1)}{P(a_v = 0)}\right) = l_{\text{MPA}}(a_v) + \sum_{c \in \mathcal{N}(v)} E_{c \rightarrow v}^{(T)}. \quad (15)$$

Finally, the BP algorithm will regard user v as asleep if $l_{\text{BP}}(a_v) < 0$ and remove it out of previously estimated active user set $\hat{\mathcal{U}}_{ac}^{\mathbf{a}}(\hat{\mathbf{I}})$. In this case, current factor graph will be reconstructed accordingly.

IV. PAYLOAD DATA DECODING

The classical MPA [27] is employed to realize the payload data decoding of all active users. The factor graph required for implementing MPA algorithm is the same as that used in Section III.D, i.e. it can directly leverage \mathbf{S}_{BP} . Without loss of generality, let us focus on the decoding of the k^{th} transmitted symbol of every active user. Accordingly, the object of MPA is to estimate the probability of $P(\mathbf{x}_u[k] = \mathcal{X}_u[m])$ for every $u \in \hat{\mathcal{U}}_{ac}^{\mathbf{a}}(\hat{\mathbf{I}})$ and $m \in [0, M]$, where $\mathbf{x}_u[k]$ is defined in Section II, rightly before (1), $\mathcal{X}_u[m]$ denotes the m^{th} legitimate symbol in the alphabet of user u , particularly, $\mathcal{X}_u[0]$ is a zero symbol. Let $E_{c \rightarrow v}^{(i)}(\mathcal{X}_v[m])$ denotes the extrinsic information of $P(\mathbf{x}_v[k] = \mathcal{X}_v[m])$ transmitted from check node c to variable node v in the i^{th} MPA iteration. Let $E_{v \rightarrow c}^{(i)}(\mathcal{X}_v[m])$ denote that transmitted from variable node v to check node c . Hence, the implementation of our MPA could be summarized as repeats of following equations.

$$E_{c \rightarrow v}^{(i)}(\mathcal{X}_v[m]) = \sum_{\substack{m' \in [0:M] \\ v' \in \mathcal{N}(c) \setminus \{v\}}} \exp\left(-\frac{1}{2\delta^2} \|\mathbf{y}_k[c] - \sum_{v' \in \mathcal{N}(c) \setminus \{v\}} \mathbf{S}[c, v'] \mathcal{X}_{v'}[m'] - \mathcal{X}_v[m]\|^2\right) \times \prod_{v' \in \mathcal{N}(c) \setminus \{v\}} E_{v' \rightarrow c}^{(i-1)}(\mathcal{X}_{v'}[m']), \quad (16)$$

$$E_{v \rightarrow c}^{(i)}(\mathcal{X}_v[m]) = \prod_{c' \in \mathcal{N}(v) \setminus \{c\}} E_{c' \rightarrow v}^{(i-1)}(\mathcal{X}_{v'}[m]), \quad (17)$$

Since the factor graph used in MPA is the same as that in Section III.D, check node c and variable node v involved in (16-17) will have the same range as that mentioned in Section III.D, i.e. we have $c \in \{l | \mathbf{I}[l] = 1\}$ and $v \in \hat{\mathcal{U}}_{ac}^{\mathbf{a}}(\hat{\mathbf{I}})$. According to the same spirit, the notations of $\mathcal{N}(c)$, $\mathcal{N}(v)$, $\mathcal{N}(c) \setminus \{v\}$, $\mathcal{N}(v) \setminus \{c\}$ remain their definitions specified in Section III.D.

At the last iteration of MPA, namely the T^{th} iteration, it will calculate the *a posteriori* information of every $P(\mathbf{x}_v[k] = \mathcal{X}_v[m])$ and record them in the probability matrix $\mathbf{P}_{\text{MPA}}^k$, which

could be formulated as

$$\mathbf{P}_{\text{MPA}}^k[m, v] = C_{m,v} \prod_{c \in \mathcal{N}(v)} E_{c \rightarrow v}^{(T)}(\mathcal{X}_v[m]), \quad (18)$$

where the parameter $C_{m,v}$ is invoked for constraining $\mathbf{P}_{\text{MPA}}^k[m, v] \in [0, 1]$.

As demonstrated in Fig. 2, the BP algorithm based active user identification and MPA based payload data decoding will iteratively exchange their information. During such an outer iteration, on the one hand, MPA will generate $l_{\text{MPA}}(a_v)$ that used in (14) for providing a priori information to the preceding BP based active user identification. $l_{\text{MPA}}(a_v)$ is calculated according to (19)

$$l_{\text{MPA}}(a_v) = \log\left(\frac{1 - \frac{1}{K} \sum_{k=1}^K \mathbf{P}_{\text{MPA}}^k[0, v]}{\frac{1}{K} \sum_{k=1}^K \mathbf{P}_{\text{MPA}}^k[0, v]}\right). \quad (19)$$

On the other hand, the *a posterior* information of activity state a_v , namely $l_{\text{BP}}(a_v)$ that is obtained from (15), will be input to MPA as its *a priori* information. MPA will utilize $l_{\text{BP}}(a_v)$ to initialize $E_{v \rightarrow c}^{(0)}(\mathcal{X}_v[m])$ that is involved in (16-17) as follows

$$E_{v \rightarrow c}^{(0)}(\mathcal{X}_v[m]) = \begin{cases} \frac{1}{1 + \exp(l_{\text{BP}}(a_v))}, & m = 0 \\ \frac{1}{M} \left(1 - \frac{1}{1 + \exp(l_{\text{BP}}(a_v))}\right), & 1 \leq m \leq M \end{cases} \quad (20)$$

When the outer iteration between BP algorithm and MPA is terminated, MPA will output its hard decision of k^{th} symbol transmitted from active user v . This operation could be formulated as

$$\begin{aligned} \hat{m} &= \arg \max_{0 \leq m \leq M} \mathbf{P}_{\text{MPA}}^k[m, v], \\ \hat{\mathbf{x}}_v[k] &= \mathcal{X}_v[\hat{m}], \end{aligned} \quad (21)$$

The aforementioned outer iterations between BP algorithm based active user identification and MPA based payload data decoding, as well as the inner iterations within themselves, are summarized as pseudo codes as shown in **Algorithm1**.

V. COMPLEXITY ANALYSIS

Considering the proposed two-stage iterative detection that is summarized in **Algorithm1**, its complexity is imposed mainly by the MPA based payload data decoding component. Then, the computational complexity of MPA is further dominated by the calculations that required

Algorithm 1 Two-stage iterative detection

Input: $\mathbf{y}_k, k \in [1, K], \delta^2, \hat{\mathbf{I}}, T_{\text{MPA}}, T_{\text{BP}}, T_{\text{outer}};$
Output: $\hat{\mathcal{U}}_{ac}^{\mathbf{a}}(\hat{\mathbf{I}}), \hat{\mathbf{x}}_v[k], v \in \hat{\mathcal{U}}_{ac}^{\mathbf{a}}(\hat{\mathbf{I}}), k \in [1, K];$

- 1: Estimate $\hat{\mathcal{U}}_{ac}^{\mathbf{a}}(\hat{\mathbf{I}})$ by cover decoder;
- 2: Generate factor graph based on $\mathbf{S}_{\text{BP}};$
- 3: **for** $t \in \{0 : T_{\text{outer}}\}$ **do**
- 4: **if** $t > 0$ **then**
- 5: $E_{v \rightarrow c}^{(0)}(\mathcal{X}_v[m]) = \begin{cases} \frac{1}{1 + \exp(l_{\text{BP}}(a_v))}, m = 0 \\ \frac{1}{M} \left(1 - \frac{1}{1 + \exp(l_{\text{BP}}(a_v))} \right), 1 \leq m \leq M \end{cases}$
- 6: **else**
- 7: $E_{v \rightarrow c}^{(0)}(\mathcal{X}_v[m]) = \frac{1}{M+1}, \forall v \in \hat{\mathcal{U}}_{ac}^{\mathbf{a}}(\hat{\mathbf{I}});$
- 8: **end if**
- 9: **for** $k \in \{1 : K\}$ **do**
- 10: **for** $i \in \{0 : T_{\text{MPA}}\}$ **do**
- 11: Update $E_{c \rightarrow v}^{(i)}(\mathcal{X}_v[m])$ according to (16);
- 12: Update $E_{v \rightarrow c}^{(i)}(\mathcal{X}_v[m])$ according to (17);
- 13: **end for**
- 14: $\mathbf{P}_{\text{MPA}}^k[m, v] = C_{m,v} \prod_{c \in \mathcal{N}(v)} E_{c \rightarrow v}^{(T_{\text{MPA}})}(\mathcal{X}_v[m]);$
- 15: **end for**
- 16: $l_{\text{MPA}}(a_v) = \log\left(\frac{1 - \frac{1}{K} \sum_{k=1}^K \mathbf{P}_{\text{MPA}}^k[0, v]}{\frac{1}{K} \sum_{k=1}^K \mathbf{P}_{\text{MPA}}^k[0, v]}\right);$
- 17: **for** $i \in \{0 : T_{\text{BP}}\}$ **do**
- 18: Update $E_{c \rightarrow v}^{(i)}$ according to (13);
- 19: Update $E_{v \rightarrow c}^{(i)}$ according to (14);
- 20: **end for**
- 21: $l_{\text{BP}}(a_v) = l_{\text{MPA}}(a_v) + \sum_{c \in \mathcal{N}(v)} E_{c \rightarrow v}^{(T_{\text{BP}})};$
- 22: **for** $\forall v \in \hat{\mathcal{U}}_{ac}$ **do**
- 23: **if** $l_{\text{BP}}(a_v) < 0$ **then** $\hat{\mathcal{U}}_{ac}^{\mathbf{a}}(\hat{\mathbf{I}}) = \hat{\mathcal{U}}_{ac}^{\mathbf{a}}(\hat{\mathbf{I}}) - \{v\}$
- 24: **end if**
- 25: **end for**
- 26: Update factor graph;
- 27: **end for**
- 28: **for** $k \in \{1 : K\}$ **do**
- 29: **for** $v \in \hat{\mathcal{U}}_{ac}^{\mathbf{a}}(\hat{\mathbf{I}})$ **do**
- 30: $\hat{m} = \arg \max_{0 \leq m \leq M} \mathbf{P}_{\text{MPA}}^k[m, v];$
- 31: $\hat{\mathbf{x}}_v[k] = \mathcal{X}_v[\hat{m}];$
- 32: **end for**
- 33: **end for**

by every check nodes on the factor graph. Hence, the complexity of the proposed two-stage iterative detection is determined by the degree distribution on \mathbf{S}_{BP} that introduced below (14). Accordingly, the complexity order of the proposed two-stage iterative detection is given by

$$\mathcal{C} = \mathcal{O}\left(K \sum_{w=1}^{w_r} p_w L(M+1)^w\right), \quad (22)$$

where p_w denotes the proportion of the check nodes, which have a degree of w to all check nodes on the factor graph \mathbf{S}_{BP} .

Proposition 4. *By employing a regular LDPC parity check matrix having row weight w_r , number of rows L , number of column N and girth larger than 4 as the spreading matrix \mathbf{S} and assuming that the load states \mathbf{I} is perfectly estimated, $\sum_{w=1}^{w_r} p_w (M+1)^w$ can be approximated as*

$$\sum_{w=1}^{w_r} p_w (M+1)^w \approx p_{w_1} (M+1)^{w_1} + p_{w_2} (M+1)^{w_2}, \quad (23)$$

where

$$\begin{aligned} p_{w_1} &= 1 - \lfloor \lambda w_r - \lfloor \lambda w_r \rfloor \rfloor \\ p_{w_2} &= 1 - p_{w_1} \\ w_1 &= \lfloor \lambda w_r \rfloor \\ w_2 &= w_1 + 1, \end{aligned} \quad (24)$$

and $\lfloor \cdot \rfloor$ returns the largest integer that less than or equal to its input.

Proof: See Appendix E. ■

Hence, the complexity order of the proposed two-stage iterative detection can be approximated as

$$\mathcal{C}_{\text{approx}} = \mathcal{O}(KL(p_{w_1} (M+1)^{w_1} + p_{w_2} (M+1)^{w_2})), \quad (25)$$

Compared with the detection method proposed in [24], whose complexity order is $\mathcal{O}(KL(M+1)^{w_r})$, the complexity order of our proposal is significantly reduced. In order to verify the

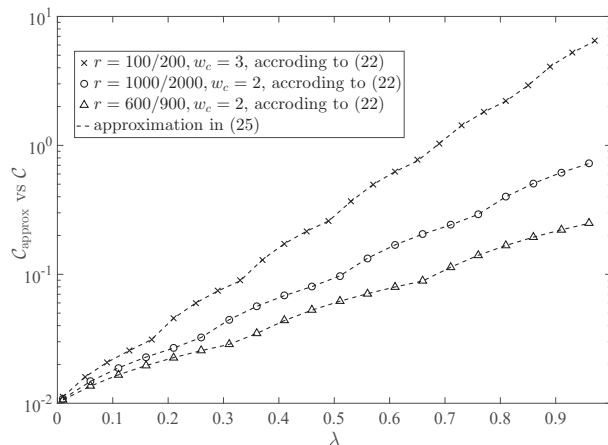


Fig. 3: Verification of (25).

TABLE II: Simulation configuration

Parameter	value
Number of coexisted users N	800
Number of time-slots L	400
Active user sparsity λ	0.02, 0.03, 0.04, 0.1, 0.5
Column Weight w_c of \mathbf{S}	2
Row Weight w_r of \mathbf{S}	4
The Value of τ in (6)	1
The Value of r^* in (12)	$\frac{1}{2}$
Constellation size M	2
Data Packet Length K	60

accuracy of our complexity order approximation, we compare $\mathcal{C}_{\text{approx}}$ obtained from (25) with \mathcal{C} obtained from (22) in Fig. 3. In order to guarantee the generality, different choices for the spreading matrix \mathbf{S} and different user sparsity λ are tested, which will further result in different factor graph \mathbf{S}_{BP} for MPA module. The detailed system configuration can be observed at the top left corner of Fig. 3. Numerical results shown in Fig. 3 confirm that replacing (22) by (25) is reasonable.

VI. SIMULATION RESULT AND DISCUSSION

In this section, the performance of active user identification and payload data decoding are demonstrated by using computer simulations. Similar to [33], when simulating the symbol error rate (SER), a symbol is regarded as correct if and only if both the user activity state and the symbol itself are correctly detected. τ_E mentioned in the Section III.C is fixed at $1.55K\delta^2$. The overloading factor which is also referred to as utilization factor in [34] is defined as $\frac{\lambda N}{L}$ [14]. Then, the system parameters are listed in TABLE II.

The impact of circle-length distribution of the spreading matrix \mathbf{S} on the false alarm performance R_{FA} is demonstrated in Fig. 4, where the number of time-slots, the number of coexisted users, and the thresholds involved in (6) are fixed to $L = 400, N = 800, \tau = 1, r^* = 0.5$, respectively. Then, different circle-length distribution could be realized by adjusting the positions of non-zero elements in \mathbf{S} . We use the notation of $[400, 0, 0]$ to represent a circle-length distribution that has 400 length-4 circles, no length-6 circles, and no length-8 circles either. For another instance, $[500, 0, 1191]$ means the constructed spreading matrix \mathbf{S} has 500 length-4

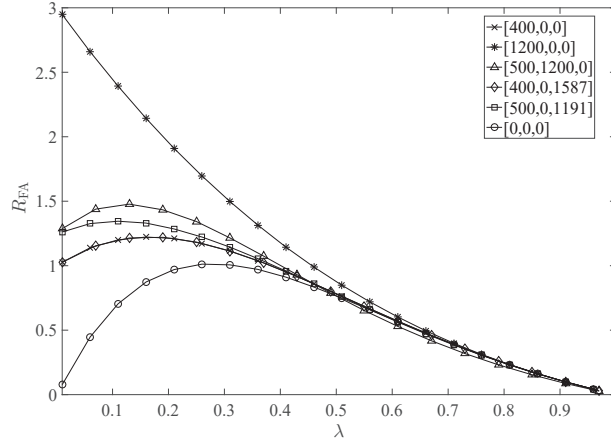


Fig. 4: Impact of circle-length distribution of spreading matrix \mathbf{S} on false alarm performance of cover decoder.

circles, no length-6 circles, and 1191 length-8 circles. The number of other circles whose length is higher than 8 is not taken into account. By comparing the curve with cross legends to that with star legends, it is clear that the growth of length-4 circles will significantly impair the false alarm performance of the cover decoder component. In contrast, the impact of length-8 circles on R_{FA} is negligible, since the curve with cross legends almost overlap the curve with diamond marks, even the later has 1587 more length-8 circles. By comparing the curve with triangle marks to that with square marks, we may conclude that false alarm performance R_{FA} may slightly degrade owing to having too many length-6 circles. Finally, the curve with circle marks confirms that it is better to remove all the short circles in the spreading matrix \mathbf{S} for improving the cover decoder performance. In this paper, the progressive edge-growth algorithm proposed in [35] is employed to optimize the circle-length distribution on the guidance obtained from Fig. 4.

Fig. 5(a) demonstrates that a smaller column weight w_c of spreading matrix \mathbf{S} will contribute a better false alarm performance of cover decoder. This phenomenon confirms the correctness of our **Proposition 2** that the growth of w_c will increase $R_{FA}(\lambda^*, w_c, r)$. The influence of extremely large w_c is shown in Fig. 5(b) In theory, (7) can not be used to predict the false alarm performance R_{FA} when $w_c > 20$. Because, the assumption adopted in (7) that the girth of the spreading matrix \mathbf{S} is always larger than 4 is no longer satisfied when w_c is too large, in fact, in this case, \mathbf{S} is

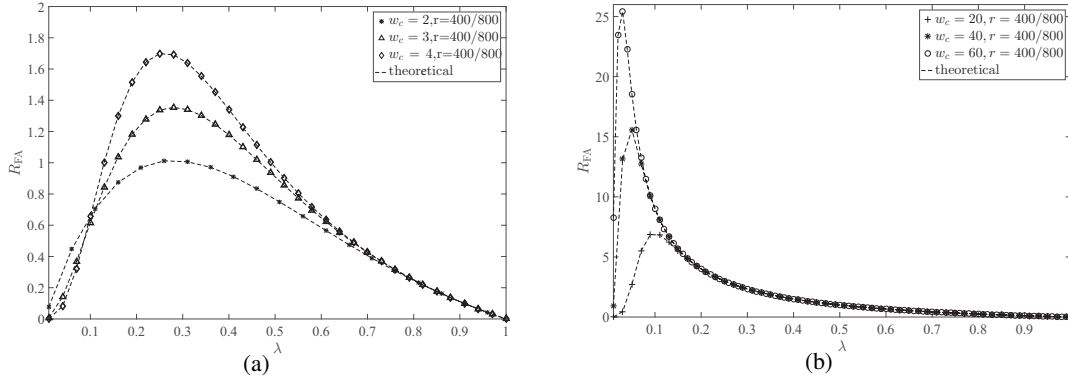


Fig. 5: Impact of column weight w_c of spreading matrix \mathbf{S} on false alarm performance of cover decoder. (a) small w_c , (b) extremely large w_c

not a sparse matrix any more. However, the simulation results in Fig. 5(b) verify that even the assumptions made in **Proposition 2** is not strictly satisfied, (7) still works well and approximates the practical performance. Furthermore, Fig. 5(b) confirms again that it is better to employ a small value of w_c .

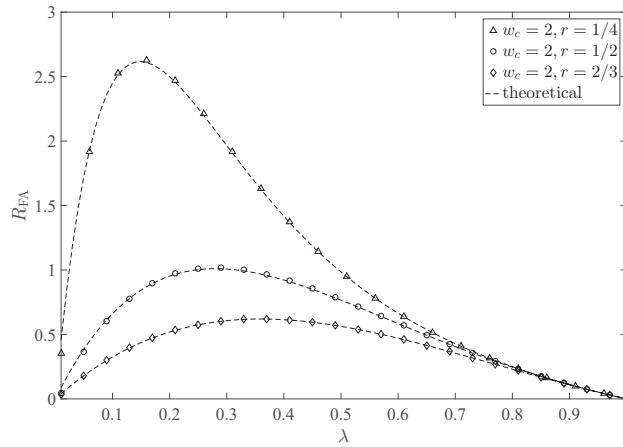


Fig. 6: Impact of ratio r of spreading matrix \mathbf{S} on false alarm performance of cover decoder.

Fig. 6 demonstrates that a larger ratio r of spreading matrix \mathbf{S} will lead to a better false alarm performance of cover decoder. This phenomenon justifies the correctness of our **Proposition 3** that the growth of r will decrease $R_{FA}(\lambda^*, w_c, r)$.

In Fig. 7, the false alarm performance R_{FA} of our proposal is compared with that of its counterpart in [21]. As can be seen from Fig. 7, the false alarm achieved by the proposed

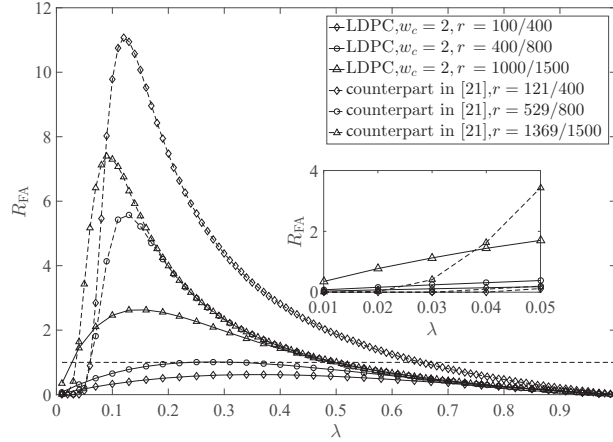


Fig. 7: False alarm performance R_{FA} comparison between the proposed protocol sequences and its counterpart in [21].

protocol sequences significantly outperforms the counterpart in [21] as long as $\lambda > 0.05$. When $0 \leq \lambda < 0.05$, the false alarm performance R_{FA} of the proposed protocol sequences is only slightly worse than the counterpart in [21].

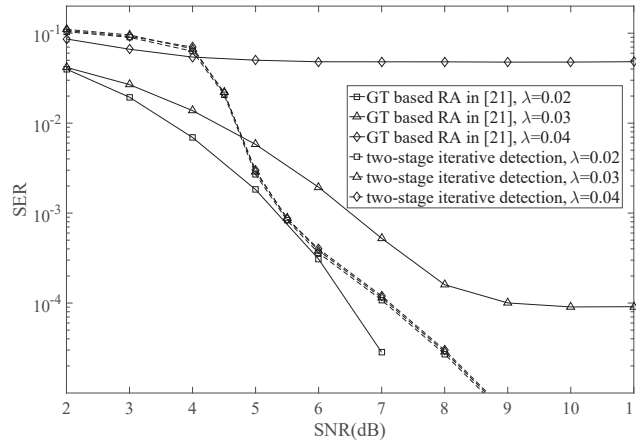


Fig. 8: SER performance comparison between our proposal and its counterpart in [21].

The SER comparison between our proposal and the counterpart in [21] is illustrated in Fig. 8. As can be seen from Fig. 8 that the SER performance of our proposal is significantly better than that of the counterpart in [21] when $\lambda \geq 0.03$. Furthermore, the SER performance of the counterpart in [21] decreases rapidly with the growth of user sparsity λ . In contrast, our

proposal is applicable to a more dense network. The reason is that the receiver in [21] will detect a collision if two or more users are sending packets in the same time-slots and these colliding packets are dropped directly. In our two-stage iteration detection architecture, these colliding packets are possibly recovered by MPA.

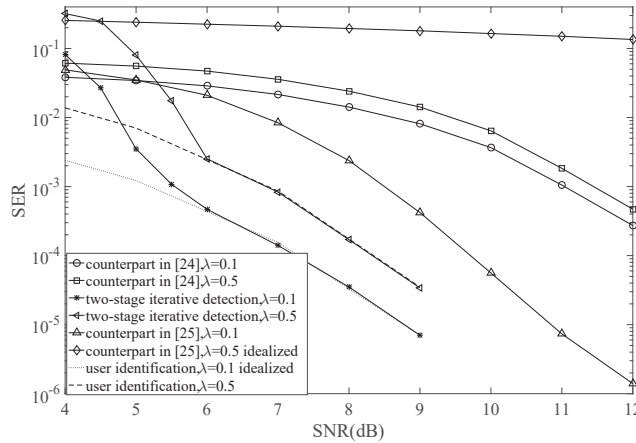


Fig. 9: The SER comparison between the counterparts in [24], [25] and the proposed two-stage iteration detection algorithm.

The SER performance of our proposal in a more dense network (e.g. $\lambda = 0.1, 0.5$) is shown in Fig. 9. As revealed in Fig. 7, the performance of counterpart [21] will dramatically degrade beyond $\lambda > 0.05$ and become significantly inferior to our proposal. Hence, in the dense access model, instead of the counterpart [21], a new detection architecture, namely “cover decoder plus MPA” detection [24] is further invoked in. In “cover decoder plus MPA” detection, firstly, the user identification is individually completed by a conventional cover decoder with the aid of a perfect estimation of load state **I**. Then, MPA introduced in Section IV is employed to process data recovery. Moreover, the counterpart in [25] is also considered. The proposed Bayesian based message passing algorithm includes two parts, namely Part (i) and Part (ii) respectively. With the output message from Part (ii), the active user identification is handled by BP and expectation propagation (EP) algorithm in Part (i). In turn, with the incoming message fed back from Part (i), the transmitted data symbols are estimated in Part (ii). As can be seen from Fig. 9 that in the low SNR region of $\text{SNR} \leq 5$ dB, the SER performance of the proposed two-stage iterative detection is worse than the counterparts in [24] and in [25]. This is due to the fact that the proposed

energy detector cannot estimate the load states \mathbf{I} at an acceptable accuracy level during this SNR region. In contrast, when $\text{SNR} \geq 6$ dB, the proposed two-stage iterative detection significantly outperforms others. This phenomenon confirms the advantage of the proposed joint detection between cover decoder and MPA, where the additional outer iterations allow them exchange extrinsic information. Furthermore, we may assume that the perfect knowledge of load states \mathbf{I} is always available at the receiver side and hence the practical energy detector employed in Fig. 2 can be removed. The other parts in Fig. 2 are remained. The resultant receiver is labeled as “idealized user identification” in Fig. 9. Obviously, it provides a performance upper bound on the proposed two-stage iterative detection. It is interesting to find that the proposed two-stage iterative detection realizes almost the same performance as that of “idealized user identification” beyond $\text{SNR} > 6$ dB. It implies that the false alarms made by cover decoder can be completely eliminated by the later BP and MPA components as long as the SNR is sufficiently large.

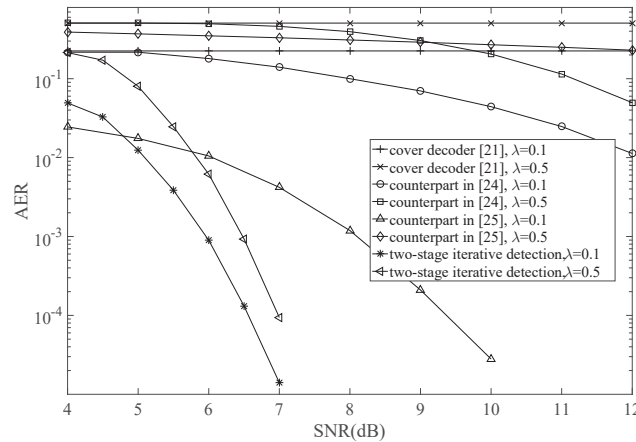


Fig. 10: Active user identification error rate (AER) performance comparison between the proposed two-stage iterative detection and its counterparts in [21], [24], [25]

The performance of active user identification of the proposed two-stage iterative detection is shown in Fig. 10. In order to fairly measure the active user identification performance, the AER metric proposed in [25] is modified to $P_{\text{AER}} = P_{\text{F}} + P_{\text{M}}$, where P_{F} denotes the probability of false detection, P_{M} denotes the probability of missed detection. Since the counterparts in [21], [24] assume the load states \mathbf{I} are perfectly known at the receiver, the P_{M} of their cover decoder is zero. Hence, their AER performances are completely determined by their P_{F} . As can be seen

from Fig. 10 that our proposal achieves the best AER performance once $\text{SNR} > 6$ dB regardless of user sparsity. Then, it is noticeable in Fig. 10 that the AER performances of other counterparts in [21], [24], [25] are constrained by a heavy user sparsity λ dramatically .

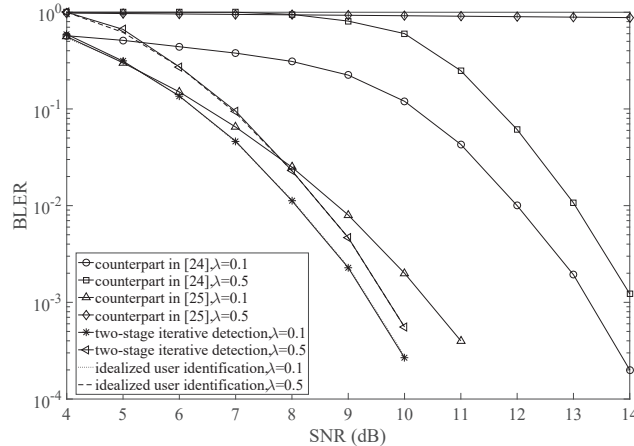


Fig. 11: Block error rate (BLER) performance comparison between the proposed two-stage iterative detection and its counterparts in [24] and [25].

The BLER performance of the proposed two-stage iterative detection is shown in Fig. 11. Again, when the user sparsity $\lambda = 0.1$, the proposed two-stage iterative detection achieves around 1.2 dB and 4 dB gain at the target of $\text{BLER} < 10^{-4}$ compared with the counterpart in [24] and the counterpart in [25], respectively. The performance gain will further grow when user sparsity $\lambda = 0.5$.

VII. CONCLUSION

In this paper, a novel transceiver architecture was designed to achieve efficient random access and reliable data transmission simultaneously. Explicit preamble transmission can be avoided by the proposed scheme. Instead, user identities are embedded into channel access patterns and controlled by protocol sequences. Consequently, the protocol sequence design becomes a critical issue. Accordingly, the columns of a LDPC parity check matrix are creatively mapped to multiple users' protocol sequences. Based on the formulation of objective functions for cover decoder, a new parity check matrix construction guideline was proposed. Then, a two-stage iterative detection was designed, which leverages group-testing algorithm, BP algorithm and

MPA. Through information transfer between these algorithms, both the active user identification and data recovery are iteratively improved. Our simulation results show that the false alarms made by the cover decoder can be almost completely corrected by the later BP and MPA components in the proposed two-stage iterative detection architecture. The practical performance of the proposed two-stage iterative detection is capable of approaching the idealized benchmark beyond $\text{SNR} \geq 7$ dB.

APPENDIX A

According to equation (24) in [36], when sparsity λ is given, the average number of false detection of spreading matrix \mathbf{S} whose girth is larger than 4 is given by

$$\frac{\sum_{\substack{\mathbf{a} \in \mathbb{B}^{N \times 1} \\ \|\mathbf{a}\|_0 = \lambda N}} |\hat{\mathcal{U}}_{\text{ac}}^{\mathbf{a}}(\mathbf{I}) - \mathcal{U}_{\text{ac}}^{\mathbf{a}}|}{\binom{N}{\lambda N}} = (1 - \lambda) \sum_{u=1}^N \prod_{l=1}^L (1 - (1 - \lambda)^{\frac{w_c}{r} - 1})^{\mathbf{S}[l,u]}. \quad (26)$$

In our design, the regular LDPC parity check matrix is employed to construct spreading matrix \mathbf{S} . Hence, (26) could be further simplified to

$$\frac{\sum_{\substack{\mathbf{a} \in \mathbb{B}^{N \times 1} \\ \|\mathbf{a}\|_0 = \lambda N}} |\hat{\mathcal{U}}_{\text{ac}}^{\mathbf{a}}(\mathbf{I}) - \mathcal{U}_{\text{ac}}^{\mathbf{a}}|}{\binom{N}{\lambda N}} = (1 - \lambda) N (1 - (1 - \lambda)^{\frac{w_c}{r} - 1})^{w_c}. \quad (27)$$

Since the size of $\mathcal{U}_{\text{ac}}^{\mathbf{a}}$ is fixed to λN , the false detection ratio R_{FA} is evaluated as

$$\begin{aligned} R_{\text{FA}}(\lambda, w_c, r) &= \frac{\sum_{\substack{\mathbf{a} \in \mathbb{B}^{N \times 1} \\ \|\mathbf{a}\|_0 = \lambda N}} |\hat{\mathcal{U}}_{\text{ac}}^{\mathbf{a}}(\mathbf{I}) - \mathcal{U}_{\text{ac}}^{\mathbf{a}}|}{\sum_{\substack{\mathbf{a} \in \mathbb{B}^{N \times 1} \\ \|\mathbf{a}\|_0 = \lambda N}} |\mathcal{U}_{\text{ac}}^{\mathbf{a}}|} \\ &= \frac{(1 - \lambda) N (1 - (1 - \lambda)^{\frac{w_c}{r} - 1})^{w_c}}{\lambda N} \\ &= \frac{1 - \lambda}{\lambda} (1 - (1 - \lambda)^{\frac{w_c}{r} - 1})^{w_c}, \end{aligned} \quad (28)$$

APPENDIX B

First, we obtain the partial derivative of $g(\lambda, w_c, r)$ with respect to w_c , which is given by

$$\frac{\partial g}{\partial w_c} = -[(1 - \lambda)^{w_c/r - 1} + w_c (1 - \lambda)^{w_c/r - 1} \ln(1 - \lambda) \frac{1}{r}], \quad (29)$$

Let $\frac{\partial g}{\partial w_c}|_{\lambda=\lambda_w} = 0$, then the solution is $\lambda_w = 1 - \exp(-\frac{r}{w_c})$. Clearly, $\frac{\partial g}{\partial w_c} \leq 0$ when $0 \leq \lambda \leq \lambda_w$ and $\frac{\partial g}{\partial w_c} \geq 0$ when $\lambda_w \leq \lambda \leq 1$.

Then, we obtain the partial derivative of $\ln(R_{\text{FA}})$ with respect to λ , which is given by

$$\frac{\partial \ln(R_{\text{FA}})}{\partial \lambda} = \frac{-1}{\lambda(1-\lambda)} + \frac{w_c(\frac{w_c}{r} - 1)(1-\lambda)^{\frac{w_c}{r}-2}}{1 - (1-\lambda)^{\frac{w_c}{r}-1}}, \quad (30)$$

Substituting λ_w to λ , then (30) becomes

$$\begin{aligned} \frac{\partial \ln(R_{\text{FA}})}{\partial \lambda}|_{\lambda=\lambda_w} &= \frac{-1}{e^{-\frac{r}{w_c}}(1-\lambda)} + \frac{w_c(\frac{w_c}{r} - 1)(e^{-\frac{r}{w_c}})^{\frac{w_c}{r}-2}}{1 - (e^{-\frac{r}{w_c}})^{\frac{w_c}{r}-1}} \\ &= \frac{e^{\frac{2r}{w_c}}}{(e - e^{\frac{r}{w_c}})(1 - e^{\frac{r}{w_c}})} k(t), \end{aligned} \quad (31)$$

where $0 < t = \frac{r}{w} < 1$, $k(t) = (e - e^t) + w_c(\frac{1}{t} - 1)(1 - e^t)$. Let $h(t) = (e - e^t) + 2(\frac{1}{t} - 1)(1 - e^t)$ and $k(t) \leq h(t)$.

The derivative of $h(t)$ can be written as

$$\begin{aligned} \frac{dh(t)}{dt} &= \frac{-2}{t^2} + e^t\left(\frac{2}{t^2} - \frac{2}{t} + 1\right) \\ &= \frac{-2}{t^2} + \left(1 + t + \frac{t^2}{2} + \mathcal{O}(t^2)\right)\left(\frac{2}{t^2} - \frac{2}{t} + 1\right) \\ &\geq \frac{-2}{t^2} + \left(1 + t + \frac{t^2}{2}\right)\left(\frac{2}{t^2} - \frac{2}{t} + 1\right) \\ &= \frac{t^2}{2} > 0, \end{aligned} \quad (32)$$

Hence, $k(t) < h(1) = 0$. Consequently, $\frac{\partial \ln(R_{\text{FA}})}{\partial \lambda}|_{\lambda=\lambda_w} > 0$. Hence, $R_{\text{FA}}(\lambda, w_c, r)$ is a concave function of λ while fixing w_c and r . It implies $\lambda_w < \lambda^*$.

Finally, $\frac{\partial g}{\partial w_c}|_{\lambda=\lambda^*} \geq 0$ is obtained. This result reveals that the bigger w_c is, the bigger $g(\lambda^*, w_c, r)$ is. The proof is accomplished.

APPENDIX C

Observe the optimization problem in (10) and (8) that the constraint C_3 is guaranteed as long as C_4 is true. It implies the set of w_c that satisfies (10) must also satisfies (8). Let w_{c,C_4}^* and w_{c,C_3}^* denotes the optimal w_c for (10) and for (8), respectively. Obviously, w_{c,C_4}^* is an upper bound on w_{c,C_3}^* , i.e. $w_{c,C_4}^* \geq w_{c,C_3}^*$.

Based on **Proposition 2**, we obtain that for any given τ , w_{c,C_4}^* is always 2. Owing to the constraint C_1 , w_{c,C_3}^* is also 2. Hence, the fact that the problem in (10) has the same optimal solution of w_c as (8) is proved.

APPENDIX D

According to the expression of R_{FA} , the partial derivative of R_{FA} with respect to r is given by

$$\frac{\partial R_{\text{FA}}}{\partial r} = \frac{w_c^2(1-\lambda)^{w_c/r} \log(1-\lambda)}{\lambda r^2} (1 - (1-\lambda)^{w_c/r-1})^{w_c-1}. \quad (33)$$

Obviously, $(1 - (1-\lambda)^{w_c/r-1}) \geq 0$, $\log(1-\lambda) \leq 0$. Hence, $\frac{\partial R_{\text{FA}}}{\partial r} \leq 0$. It implies that the bigger r is, the smaller R_{FA} is. The proof is accomplished.

APPENDIX E

Let \mathcal{S}_u^l denote the user set who possibly interferes with user u on the l^{th} time slot, i.e. $\mathbf{S}[l, u'] = 1, 1 \leq u' \neq u \leq N$. Since the girth length of \mathbf{S} is larger than or equal to 6, we have $\mathcal{S}_u^{l_1} \cap \mathcal{S}_u^{l_2} = \emptyset$, while $l_1 \neq l_2$, $\mathbf{S}[l_1, u] = \mathbf{S}[l_2, u] = 1$. Then, let random variable W_u^l denote the size of \mathcal{S}_u^l . According to [36], the values of the random variables $W_u^l, 1 \leq l \leq L, \mathbf{S}[l, u] = 1$ are independent.

Obviously, the degree of any check node in the factor graph $\mathbf{S}[:, \mathcal{U}_{ac}^a]$ is dominated by size of the set $\mathcal{S}_u^l \cup \{u\}, \mathbf{S}[l, u] = 1$. Hence, the expectation of the degree of the l^{th} check node d_c^l can be formulated as

$$E[d_c^l] = E[W_u^l] + E[a_u]. \quad (34)$$

In our scenario, any column in the spreading matrix \mathbf{S} has a probability λ to be added into the spreading matrix of active user set $\mathbf{S}[:, \mathcal{U}_{ac}^a]$. Hence, W_u^l obeys to a binomial distribution $B(w_r - 1, \lambda)$. Hence, $E[W_u^l] = \lambda(w_r - 1)$. Furthermore, we have $E[a_u] = \lambda$. According to (34), $E[d_c^l] = \lambda w_r$. Moreover, the values of d_c^l must be an integer. Hence, the value of d_c^l could be a random integer whose value is $w_1 = \lfloor \lambda w_r \rfloor$ with a probability of $p_{w_1} = 1 - (\lambda w_r - \lfloor \lambda w_r \rfloor)$ and $w_2 = w_1 + 1$ with a probability of $1 - p_{w_1}$. The proof is accomplished.

REFERENCES

- [1] E. Au, "A short update on 3GPP release 16 and release 17 [standards]," *IEEE Vehicular Technology Magazine*, vol. 15, no. 2, pp. 160–160, 2020.

- [2] 3GPP, IMT-2020 connection density evaluation results (mMTC), R1-1808866, Aug. 2018.
- [3] C. Bockelmann, N. K. Pratas, G. Wunder, S. Saur, M. Navarro, D. Gregoratti, G. Vivier, E. De Carvalho, Y. Ji, Č. Stefanović *et al.*, “Towards massive connectivity support for scalable mMTC communications in 5g networks,” *IEEE access*, vol. 6, pp. 28 969–28 992, 2018.
- [4] 3GPP, IMT-2020 self evaluation: mMTC coverage, data rate, latency & battery life, R1-1905187, Apr. 2019.
- [5] I. C. S. L. S. Committee *et al.*, “IEEE standard for information technology-telecommunications and information exchange between systems-local and metropolitan area networks-specific requirements part 11: Wireless LAN medium access control (MAC) and physical layer (PHY) specifications,” *IEEE Std 802.11[^]*, 2007.
- [6] Z. Chen, F. Sotiriou, and W. Yu, “Sparse activity detection for massive connectivity,” *IEEE Transactions on Signal Processing*, vol. 66, no. 7, pp. 1890–1904, 2018.
- [7] L. Liu and W. Yu, “Massive connectivity with massive MIMO-Part I: Device activity detection and channel estimation,” *IEEE Transactions on Signal Processing*, vol. 66, no. 11, pp. 2933–2946, 2018.
- [8] L. Liu, E. G. Larsson, W. Yu, P. Popovski, C. Stefanovic, and E. De Carvalho, “Sparse signal processing for grant-free massive connectivity: A future paradigm for random access protocols in the internet of things,” *IEEE Signal Processing Magazine*, vol. 35, no. 5, pp. 88–99, 2018.
- [9] Y. Polyanskiy, “A perspective on massive random-access,” in *2017 IEEE International Symposium on Information Theory (ISIT)*. IEEE, 2017, pp. 2523–2527.
- [10] O. Ordentlich and Y. Polyanskiy, “Low complexity schemes for the random access gaussian channel,” in *2017 IEEE International Symposium on Information Theory (ISIT)*. IEEE, 2017, pp. 2528–2532.
- [11] A. K. Pradhan, V. K. Amalladinne, K. R. Narayanan, and J.-F. Chamberland, “Polar coding and random spreading for unsourced multiple access,” in *ICC 2020-2020 IEEE International Conference on Communications (ICC)*. IEEE, 2020, pp. 1–6.
- [12] A. Pradhan, V. Amalladinne, A. Vem, K. R. Narayanan, and J.-F. Chamberland, “A joint graph based coding scheme for the unsourced random access gaussian channel,” in *2019 IEEE Global Communications Conference (GLOBECOM)*. IEEE, 2019, pp. 1–6.
- [13] M. Zheng, Y. Wu, and W. Zhang, “Polar coding and sparse spreading for massive unsourced random access,” *arXiv preprint arXiv:2007.05739*, 2020.
- [14] O. O. Oyerinde, “Compressive sensing algorithms for multiuser detection in uplink grant free NOMA systems,” in *2019 IEEE 89th Vehicular Technology Conference (VTC2019-Spring)*. IEEE, 2019, pp. 1–6.
- [15] N. Y. Yu, “Binary golay spreading sequences and reed-muller codes for uplink grant-free NOMA,” *IEEE Transactions on Communications*, 2020.
- [16] Y. Liu, L.-L. Yang, and L. Hanzo, “Joint user-activity and data detection for grant-free spatial-modulated multi-carrier non-orthogonal multiple access,” *IEEE Transactions on Vehicular Technology*, vol. 69, no. 10, pp. 11 673–11 684, 2020.
- [17] S. Adnan, Y. Fu, J. A. Bhutto, J. N. U. Rehman, R. A. Wagan, and A. Ghulam, “An improved CoSaMP multiuser detection for uplink grant free NOMA system.”
- [18] D. Abed and A. Medjouri, “CS-based near-optimal MUD for uplink grant-free NOMA,” *Wireless Personal Communications*, pp. 1–10, 2021.
- [19] N. Y. Yu, “Multiuser activity and data detection via sparsity-blind greedy recovery for uplink grant-free NOMA,” *IEEE Communications Letters*, vol. 23, no. 11, pp. 2082–2085, 2019.

- [20] S. Li, L. Xiao, and T. Jiang, "An efficient matching pursuit based compressive sensing detector for uplink grant-free NOMA," *IEEE Transactions on Vehicular Technology*, vol. 70, no. 2, pp. 2012–2017, 2021.
- [21] H. A. Inan, S. Ahn, P. Kairouz, and A. Ozgur, "A group testing approach to random access for short-packet communication," in *2019 IEEE International Symposium on Information Theory (ISIT)*, 2019, pp. 96–100.
- [22] S. Zahidah and A. Barra, "The construction of disjunct matrix for non-adaptive group testing," in *Journal of Physics: Conference Series*, vol. 1028, no. 1. IOP Publishing, 2018, p. 012116.
- [23] P. Sasmal, S. S. Thoota, and C. R. Murthy, "Disjunct matrices for compressed sensing," in *ICASSP 2019-2019 IEEE International Conference on Acoustics, Speech and Signal Processing (ICASSP)*. IEEE, 2019, pp. 4888–4892.
- [24] H. Zhu and G. B. Giannakis, "Exploiting sparse user activity in multiuser detection," *IEEE Transactions on Communications*, vol. 59, no. 2, pp. 454–465, 2010.
- [25] Y. Zhang, Z. Yuan, Q. Guo, Z. Wang, J. Xi, and Y. Li, "Bayesian receiver design for grant-free noma with message passing based structured signal estimation," *IEEE Transactions on Vehicular Technology*, vol. 69, no. 8, pp. 8643–8656, 2020.
- [26] J. Van De Beek and B. M. Popovic, "Multiple access with low-density signatures," in *GLOBECOM 2009-2009 IEEE Global Telecommunications Conference*. IEEE, 2009, pp. 1–6.
- [27] R. Hoshyar, F. P. Wathan, and R. Tafazolli, "Novel low-density signature for synchronous CDMA systems over AWGN channel," *IEEE Transactions on Signal Processing*, vol. 56, no. 4, pp. 1616–1626, 2008.
- [28] S. Chen, B. Ren, Q. Gao, S. Kang, S. Sun, and K. Niu, "Pattern division multiple access-A novel nonorthogonal multiple access for fifth-generation radio networks," *IEEE Transactions on Vehicular Technology*, vol. 66, no. 4, pp. 3185–3196, 2016.
- [29] S. Zhang, X. Xu, L. Lu, Y. Wu, G. He, and Y. Chen, "Sparse code multiple access: An energy efficient uplink approach for 5g wireless systems," in *2014 IEEE Global Communications Conference*. IEEE, 2014, pp. 4782–4787.
- [30] J. Zhang, L. Chen, P. T. Boufounos, and Y. Gu, "On the theoretical analysis of cross validation in compressive sensing," in *2014 IEEE International Conference on Acoustics, Speech and Signal Processing (ICASSP)*. IEEE, 2014, pp. 3370–3374.
- [31] R. T. Marler and J. S. Arora, "Survey of multi-objective optimization methods for engineering," *Structural and multidisciplinary optimization*, vol. 26, no. 6, pp. 369–395, 2004.
- [32] X. Bian, Y. Mao, and J. Zhang, "Supporting more active users for massive access via data-assisted activity detection," in *ICC 2021-IEEE International Conference on Communications*. IEEE, 2021, pp. 1–6.
- [33] S. Jiang, X. Yuan, X. Wang, C. Xu, and W. Yu, "Joint user identification, channel estimation, and signal detection for grant-free NOMA," *IEEE Transactions on Wireless Communications*, vol. 19, no. 10, pp. 6960–6976, 2020.
- [34] A. T. Abebe and C. G. Kang, "Multi-sequence spreading random access (MSRA) for compressive sensing-based grant-free communication," *IEEE Transactions on Communications*, vol. 69, no. 11, pp. 7531–7543, 2021.
- [35] X.-Y. Hu, E. Eleftheriou, and D. Arnold, "Regular and irregular progressive edge-growth tanner graphs," *IEEE Transactions on Information Theory*, vol. 51, no. 1, pp. 386–398, 2005.
- [36] M. Mézard and C. Toninelli, "Group testing with random pools: Optimal two-stage algorithms," *IEEE Transactions on Information Theory*, vol. 57, no. 3, pp. 1736–1745, 2011.